PCCP

Detection of remote proton-nitrogen correlations by ^{1}H-detected ^{14}N overtone solid-state NMR at fast MAS

Journal:	*Physical Chemistry Chemical Physics*
Manuscript ID	CP-ART-01-2022-000155.R1
Article Type:	Paper
Date Submitted by the Author:	02-Mar-2022
Complete List of Authors:	Duong, Nghia Tuan; Riken Yokohama Institute, RIKEN-JEOL Collaboration Center Nishiyama, Yusuke; Riken Yokohama Institute

SCHOLARONE™
Manuscripts

Detection of remote proton-nitrogen correlations

by [1]H-detected ^{14}N overtone solid-state NMR at fast MAS

Nghia Tuan Duong[1*], Yusuke Nishiyama[1,2*]

[1] Nano-Crystallography Unit, RIKEN-JEOL Collaboration Center, Yokohama, Kanagawa 230-0045, Japan

[2] JEOL RESONANCE Inc., Musashino, Akishima, Tokyo 196-8558, Japan

* Corresponding authors. Email: duongtuannghia86@gmail.com, yunishiy@jeol.co.jp

Abstract

Detecting proton and nitrogen correlation in solid-state nuclear magnetic resonance (NMR) is important for the structural determinations of biological and chemical systems. Recent advances on proton-detection at fast magic-angle spinning approaches have facilitated the detection of ^{1}H-^{14}N correlations by solid-state NMR. However, observing remote ^{1}H-^{14}N correlations by these approaches is still a challenge, especially for ^{14}N sites having large quadrupolar couplings. To address this issue, we introduce the ^{1}H-^{14}N overtone continuous wave rotational-echo saturation-pulse double-resonance (^{1}H-^{14}N OT CW-RESPDOR) sequence. Unlike regular 2D correlation experiments where the indirect dimension is recorded in the time domain, the ^{1}H-^{14}N OT CW-RESPDOR experiment is directly observed in the frequency domain. A set of ^{1}H-^{14}N OT CW-RESPDOR filtered ^{1}H spectra is recorded at varying ^{14}N OT frequency. Thanks to the selective nature of the ^{14}N OT pulse, the filtered ^{1}H spectra appear only if ^{14}N OT frequency hits the positions of ^{14}N OT central band or one of the spinning sidebands. This set of filtered ^{1}H spectra represents a 2D ^{1}H-^{14}N OT correlation map. We have also investigated the optimizable parameters for CW-RESPDOR and figured out that these parameters are not strictly needed for our working magnetic field of 14.1 T. Hence, the experiment is easy to setup and requires almost no optimization. We have demonstrated the experimental feasibility of ^{1}H-^{14}N OT CW-RESPDOR on monoclinic L-histidine and L-alanyl L-alanine. The remote ^{1}H-^{14}N correlations have been efficiently detected no matter how large the ^{14}N quadrupolar interaction is and agree with the crystal structures. In addition, based on the remote ^{1}H-^{14}N correlations from the non-protonated ^{14}N site of L-histidine, we can unambiguously distinguish the orthorhombic and monoclinic forms.

1. Introduction

Proton and nitrogen present in various biological and chemical systems, thus detecting their correlations can reveal crucial structural information. While proton-nitrogen correlation between covalently bonded NH pair provides direct assignment of NH proton, long-range NH correlation is crucial for sequential assignments and structural analysis. The notable example is found in HMBC to probe multi-bond correlations in solution NMR[1] and ^{1}H-detected HETCOR with long contact time to probe spatial proximal nuclei in solid-state NMR[2]. Although ^{15}N is widely used in nuclear magnetic resonance (NMR) due to its simplicity of spin-1/2, poor sensitivity owing to small natural abundance of ^{15}N (<0.4%) prevent ^{15}N NMR from daily observation. On the other hand, despite the high natural abundance of ^{14}N (>99.6%), the direct detection of ^{14}N is considered difficult. This is because ^{14}N has a quadrupolar moment and spin-1. Owing to these characteristics, the fundamental transitions of ^{14}N are severely broadened by the quadrupolar interaction, causing the dramatic loss of sensitivity. Two independent groups had broken the barrier and paved a way to ^{14}N NMR using an ingenious idea of indirect detection via a handier spin-1/2, such as ^{13}C[3–5] or ^{1}H[6–10]. The most common method to observe correlation between ^{1}H and ^{14}N is the two-dimensional ^{1}H/{^{14}N} dipolar-based heteronuclear multiple quantum coherences (2D D-HMQC) experiment at fast magic-angle spinning (MAS) condition ($v_R \geq 50$ kHz, where v_R represents the MAS frequency)[11]. Several ^{14}N excitation/reconversion schemes[12–18] or de-/recoupling sequences[19–22] have been studied to improve the performance of D-HMQC. Other methods have also been developed, such as double cross-polarization (DCP)[23] and TRAPDOR-HMQC (or T-HMQC)[24–26]. D-HMQC, DCP, and T-HMQC experiments have found applications on many biological, chemical, and pharmaceutical solids[27–36].

The detection of one-bond ^{1}H-^{14}N correlation by the three experiments above is simple and highly efficient. It typically takes only several minutes to hours. However, it is still a challenge to observe remote ^{1}H-^{14}N correlations, especially for ^{14}N having a large quadrupolar coupling (C_Q) due to a poor efficiency. We take an example of correlations among ^{1}Hs and a non-protonated ^{14}N site of L-histidine compound (C_Q of about 3 MHz). For T-HMQC, it fails to detect these correlations[24]. For D-HMQC, the detection is feasible provided that long recoupling time is used because the non-protonated ^{14}N site is remote to ^{1}H sites, thus small ^{1}H-^{14}N dipolar couplings. However, the price to pay is the loss of sensitivity owing to the relaxation decay (T_2') during ^{1}H-^{14}N dipolar recoupling blocks, making experiments lengthy. For DCP, remote ^{1}H-^{14}N correlations were observed for L-histidine[23]; however, the use of long contact time (up to 6.4 ms) generated relayed ^{1}H-^{14}N correlations within the compound due to the spin diffusion among ^{1}Hs during spin-lock[37]. This is of impractical use for structural investigations. In addition, these

three methods require demanding optimizations with a prior knowledge of ^{14}N shifts. Even knowing ^{14}N shifts, additional point needs to be considered for D-HMQC. We assume a system with two ^{14}N sites. The on-resonance offset on one ^{14}N site causes a null signal for the second site when their ^{14}N shift difference is one-fourth of v_R (v_R /4)[38]. This is caused by the non-zero evolution period for the first t_1 point to achieve rotor-synchronous ^{14}N pulses.

To address these difficulties, we present a new method for detecting remote [1]H-^{14}N correlations with [1]H-^{14}N overtone continuous wave rotational-echo saturation-pulse double-resonance ([1]H-^{14}N OT CW-RESPDOR) sequence[39–41]. The RESPDOR sequence have been widely used to detect the spatial proximity/interaction between ^{1}H and a quadrupolar nucleus such as [14]N[42,43], [63]Cu[44], [65]Zn[45], [71]Ga[46], [79]Br[47], and [95]Mo[48]. Here we use the ^{14}N OT ($|\Delta m|$ = 2) transitions[49–55] instead of the fundamental ^{14}N transitions ($|\Delta m|$ = 1), where m denotes the energy level. A number of methods for detecting [1]H-^{14}N OT correlations have been studied[56–59]. The main advantage of ^{14}N OT is devoid of the first-order quadrupolar interaction. However, the relatively low sensitivity is an issue due to the small transition probability of ^{14}N OT. Furthermore, the limited bandwidth of ^{14}N OT prevents the simultaneous detection of [1]H-^{14}N OT correlations when a system consists of more than one ^{14}N site. In the current experiment, a set of [1]H-^{14}N OT CW-RESPDOR filtered ^{1}H spectra is recorded at varying ^{14}N OT frequencies. Such frequency sweep approach was used to indirectly record the [27]Al spectrum for zeolites with ^{1}H/[27]Al TRAPDOR[60] and REAPDOR[61]. However, the unique feature of [1]H-^{14}N OT CW-RESPDOR is that the limited bandwidth of ^{14}N OT pulses leads to selective observation of ^{1}H signals in the vicinity of on-resonant ^{14}N OT species. The arrayed ^{1}H spectra give 2D [1]H-^{14}N OT correlations. The details of the working principle of the approach and its advantages over the existing sequences are discussed. Herein, we demonstrate the applicability of our method on the two stable crystalline forms of L-histidine compound: orthorhombic (Hist-A) and monoclinic (Hist-B) as well as L-alanyl L-alanine (AlaAla). The C_Q values of the three samples are in 1 – 4 MHz range.

2. Pulse sequence description

Fig. 1 presents the [1]H-^{14}N OT CW-RESPDOR sequence. The [1]H-^{14}N dipolar coupling, recovered by the SR4 recoupling block[19], is refocused by the [1]H π pulse in the middle of the sequence without a ^{14}N OT irradiation, giving S_0 signal. However, the refocusing is prevented with a ^{14}N OT irradiation. It introduces the dipolar dephasing or RESPDOR/REDOR decay, giving S' signal. The signal difference ($S_0 - S'$) measures the extent of the RESPDOR effect. Our sequence works by recording S_0 once as S_0 is immune to the [14]N

4

OT frequency but recording S' at each ^{14}N OT shift for the filtered ^{1}H spectra ($S_0 - S'$). It should be mentioned that the effect of long-term instability can be reduced by collecting S_0 and S' alternatively. This doubles the measurement time but can lead to less t_1-noise. While we use the same number of scans to record both S_0 and S' throughout the work, the ratio of number of scans may be optimized to maximize the sensitivity per unit of time. Thanks to the selective nature of the ^{14}N OT pulse, the RESPDOR effect or the ($S_0 - S'$) signal is appreciable only when the ^{14}N OT frequency is close to either central band or spinning sidebands (SSBs) of the ^{14}N OT peak of interest. By collecting these filtered ^{1}H spectra, we obtained a 2D correlation map, where the horizontal axis shows the ^{1}H spectrum while the vertical axis shows an array of ^{14}N OT shifts with the corresponding ($S_0 - S'$) intensities. It should be noted that the success of our method is completely based on the limited bandwidth of the ^{14}N OT pulse.

Our method offers a number of advantages compared to D-/ T-HMQC and DCP. First, shorter recoupling time (τ_{mix}) is needed to detect a remote ^{1}H-^{14}N correlation using ^{14}N OT as compared to ^{14}N. This is because RESPDOR signals with the ^{14}N OT frequency dephase two-times faster than that with the fundamental ^{14}N frequency[62]. Such shorter τ_{mix} helps to reduce the relaxation decay, thus promoting remote ^{1}H-^{14}N correlations with improved sensitivities. Second, unlike DCP, ^{1}H-^{14}N relayed correlations are avoided because ^{1}H-^{1}H spin diffusion is well suppressed during ^{1}H-^{14}N SR4 recoupling. Third, the prior knowledge on ^{14}N shifts for optimization is not required. Different from D-HMQC, DCP, and T-HMQC experiments where the experimental setup and optimization heavily depend on the ^{14}N shift, our method is free from this dependence because the ^{14}N OT shift is varied. The optimizable parameters for CW-RESPDOR are τ_{mix} and τ_{CW}, but we show later that their optimizations are not strictly needed. Fourth, D-HMQC and CW-RESPDOR allow the detection of remote ^{1}H-^{14}N correlations even in the presence of close correlations since SR4 is immune to the dipolar truncation, unlike T-HMQC. Fifth, to get the absorption lineshapes in the 2D spectrum, we must phase the indirect dimension in D-HMQC experiment due to the non-zero initial t_1 evolution time, whereas this is unnecessary for CW-REPSDOR.
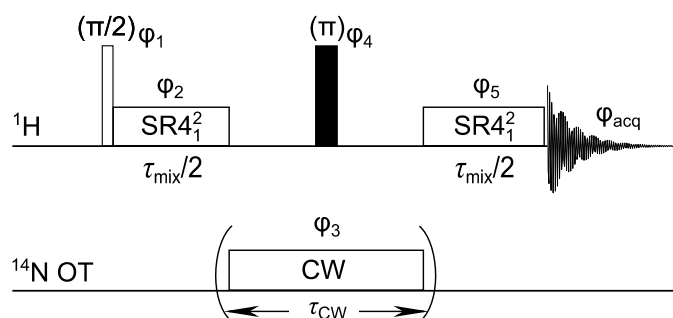
Figure 1. ^{1}H-^{14}N OT CW-RESPDOR experiment. S_0 signal is only recorded once without a ^{14}N OT irradiation whereas S' signals are recorded with each ^{14}N OT shift. A filtered ^{1}H spectrum at a specific ^{14}N OT shift is obtained by the signal difference ($S_0 - S'$). A set of filtered ^{1}H spectra at varied ^{14}N OT shift is collected for a 2D correlation map. The phase cycling is φ_1 = {3(0), 3(120), 3(240)}; $\varphi_2 = \varphi_3 = 0$; φ_4 = {0, 120, 240}; $\varphi_5 = 0$; φ_{acq} = {0, 240, 120, 240, 120, 0, 120, 0, 240}; the unit is degree ($^\circ$).

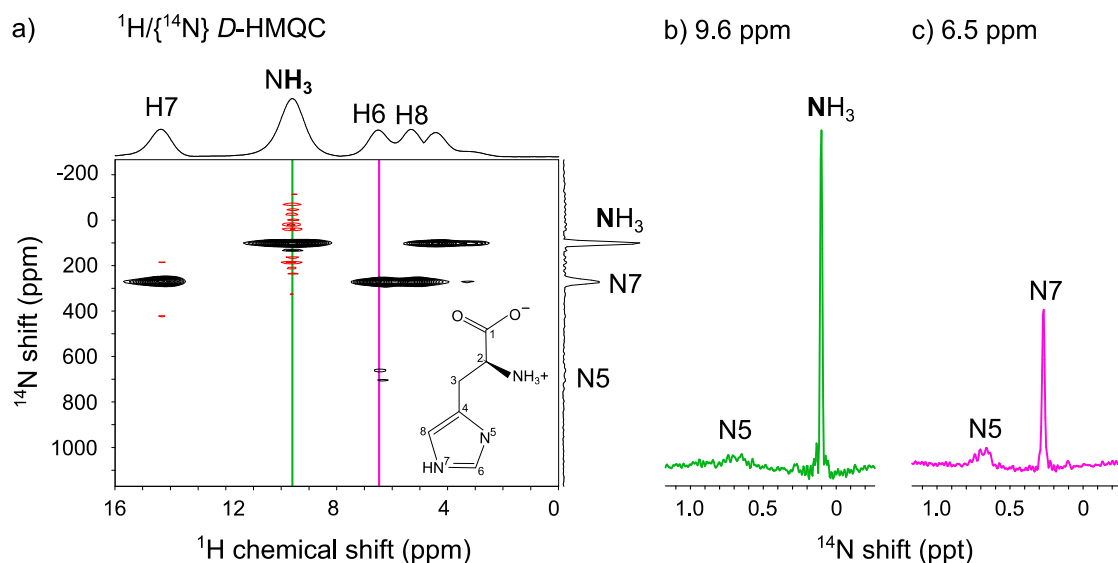# 3. Experimental

L-histidine powder was purchased from Wako Pure Chemical Industries Ltd., Japan. Hist-A and Hist-B were prepared as reported[63]. AlaAla was purchased from Sigma-Aldrich and used as received. The samples were separately packed into 1.0 mm zirconia rotors. The rotors were subsequently inserted into the 1 mm ^{1}H/X double-resonance probe for spinning at a v_R of 62.5 kHz. All NMR experiments were recorded at an ambient temperature on JNM-ECZ600R (JEOL RESONANCE Inc., Japan) at 14.1 T solid-state NMR spectrometer. The ^{1}H, ^{14}N, and ^{14}N OT Larmor frequencies are 600.0, 43.4, and 86.8 MHz, respectively. For the highest signal-to-noise ratio (S/N), the ^{14}N OT frequency was set at the second SSB (n = -2), where the "-" sign of n depends on the sense of rotation with respect to the direction of the B_0 magnetic field. The ^{14}N and ^{14}N OT shifts are referenced to NH_3 (liquid), whose ^{14}N and ^{14}N OT shift equal to 0 ppm or 0 kHz. For the experiment with ^{14}N, the ^{1}H rf-field was 243 kHz for $\pi/2$ and π pulses while for the experiments with ^{14}N OT, the corresponding value was 313 kHz. The ^{1}H rf-field for the $SR4_1^2$ recoupling sequence was fixed at $2v_R$ = 125 kHz. The ^{14}N and ^{14}N OT rf-fields were 67 and 125 kHz, respectively. Note that ^{14}N OT rf-field strength was calibrated using the heteronuclear Bloch-Siegert shift[64], thus the field strength represents the nutation rate of the virtual nucleus with the Larmor frequency of twice of the ^{14}N fundamental transitions. The recycling delays for both Hist-A and Hist-B were 5 s while that of AlaAla was 2 s. Additional experimental parameters are given in the figure captions.

4. Results and Discussions

4.1. ^{1}H/{^{14}N} D-HMQC experiment

Fig. 2a shows the 2D ^{1}H/{^{14}N} D-HMQC spectrum of Hist-B acquired at τ_{mix} of 1.536 ms (8 loops of SR4 recoupling block). The remote H6-N7 and H8-N7 correlations are clearly observed. On the other hand, the correlation between H6 and N5, which is the non-protonated ^{14}N site, is detected but it is negligible compared to the others, whereas the H8-N5 and N**H$_3$**-N5 correlations are hardly seen. We note that the correlations of H6-N7 (distances: 1.90 and 3.33 Å) and H8-N7 (distances: 2.07 and 3.13 Å) are much stronger than the H6-N5 (distances: 2.01 and 3.11 Å) despite their similar corresponding intra- and intermolecular distances. This is because of the rather small C_Q of N7 than that of N5 (shown later), causing higher excitation efficiency for the N7 site. To assess the relative intensity of the N5 site with respect to other ^{14}N sites, we extract the ^{14}N slices at, 9.6 ppm (N**H$_3$**), and 6.5 ppm (H6) (vertical line in Fig. 2a) and show them in Figs. 2b and c, respectively. In Fig. 2c, the N5 peak is visible but its intensity is weak compared to N7 as discussed above. In Fig. 2b, the N5 peak is still recognized although it is comparable to the noise level. Besides different C_Q values, the much weaker intensity of N5 peak is also due to the longer N**H$_3$**-N5 distances as compared to the bonded H-N for NH$_3$ site. We additionally performed ^{1}H/{^{14}N} D-HMQC at τ_{mix} of 0.768 ms, 1.152 ms, and 2.304 ms (corresponding to 4, 6, and 12 loops of SR4) but the intensities of N5 peak only show minor variations (see Fig. S1). In short, the regular ^{1}H/{^{14}N} D-HMQC experiment is inefficient to detect remote ^{1}H-^{14}N correlations for ^{14}N site having a large quadrupolar coupling.

Figure 2. Hist-B: a) the 2D ^{1}H/{^{14}N} D-HMQC spectrum, recorded with 128 scans, 64 t_1 points, and rotor-synchronized t_1 increment of 16.0 μs. The ^{14}N (offset and pulse length) and τ_{mix}, were set to (450 ppm

and 7 µs) and 1.536 ms, respectively. The experimental time was about 22.7 hour. The States-TPPI method was employed for the quadrature detection along the indirect dimension[65]. b,c) The extracted ^{14}N slices at ^{1}H chemical shift of b) 9.6 ppm (NH$_3$) and c) 6.5 ppm (H6) (vertical lines in a)). For a), the chemical structure of Hist-B is presented inside the 2D spectrum. The positive contour signals are presented in black while the negative ones are presented in red.
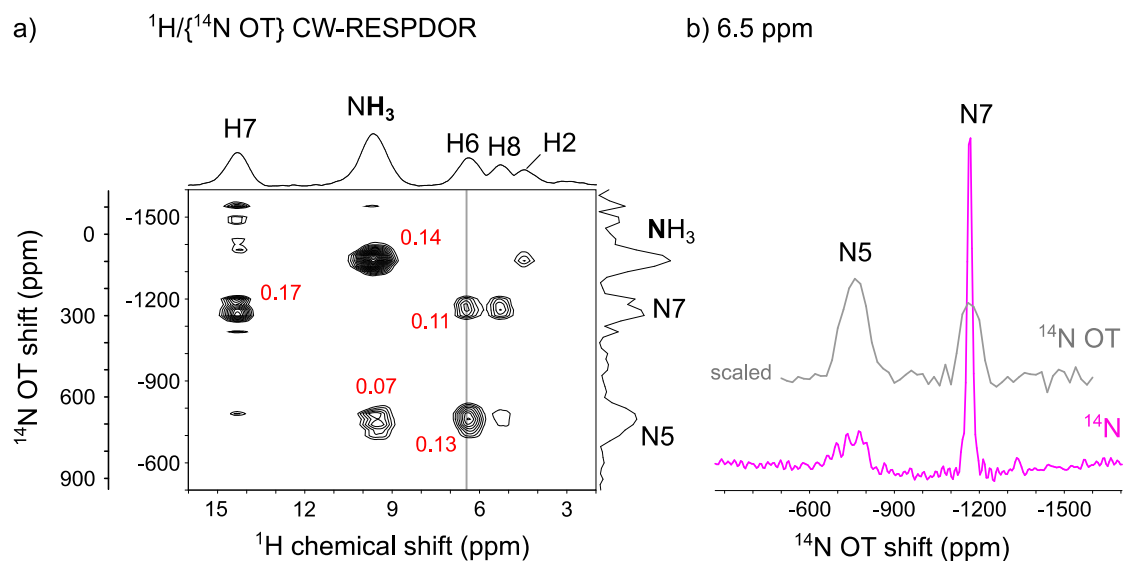
4.2. ^{1}H-^{14}N OT CW-RESPDOR experiment: Hist-B

Addressing the issue of ^{1}H/{^{14}N} D-HMQC with remote ^{1}H-^{14}N correlations for the non-protonated N5 site, we performed the ^{1}H-^{14}N OT CW-RESPDOR experiment. It is worth noting how we estimated a suitable τ_{mix}. For a bonded N-H pair with a typical distance of 1.0 Å, the ^{1}H-^{14}N OT rotational-echo double-resonance (REDOR) fractional curve reaches maximum at τ_{mix} of 0.192 ms (1 loop of SR4). We note here that the working principles of REDOR and RESPDOR for ^{14}N OT are the same; thus, they can be interchangeable. For a non-protonated N site, the distance to the nearest ^{1}H is typically about 2.0 Å, which requires τ_{mix} 8 times longer because the dipolar coupling is inversely proportional to the cube of the internuclear distance. This corresponds to τ_{mix} of 1.536 ms (8 loops of SR4). To compromise between the signal intensity and the relaxation decay, we halved τ_{mix} to 0.768 ms (4 loops of SR4). Such estimation strategy is nearly sample-independent, thus almost lifts the optimization for τ_{mix}.

Fig. 3a shows the ^{1}H-^{14}N OT correlation map of Hist-B acquired at τ_{mix} of 0.768 ms (4 loops of SR4) and τ_{CW} of 0.128 ms. We clearly observe the ^{1}H-^{14}N correlations of the N5 site including N**H$_3$**-N5, H6-N5, and H8-N5. It should be noted that even the H8-N5 correlation where the closest intermolecular distance is 2.69 Å as well as the NH$_3$-N5 correlation appear. We remind that these two correlations are hardly seen in D-HMQC above despite the experimental time of up to 23 hours. These remote correlations to the non-protonated N5 site are consistent with the crystal structure. In order to evaluate the detection efficiency, we extracted the ^{14}N OT shift array at ^{1}H chemical shift of 6.5 ppm (H6, vertical line in Fig. 3a) and compared its relative intensity with the ^{14}N slice in Fig. 2c. We note that it is not straightforward to make a fair comparison between D-HMQC and RESPDOR experiment since the efficiency of ^{1}H-^{14}N polarization transfer/dephasing highly depends on the employed recoupling times, ^{1}H-^{14}N dipolar interaction, ^{14}N quadrupolar interactions as well as the relaxation time of different spins. This makes the comparison somewhat qualitative. We scaled the intensity of the extracted ^{14}N OT shift array so that its noise is comparable to that of ^{14}N slice for the ease of comparison. Furthermore, we acquired the ^{14}N and ^{14}N OT spectra with similar resolution, namely about 22.5 ppm (64 points in 62.5

kHz bandwidth) and 20 ppm, respectively. With four times zero-filling used in the $^1H/\{^{14}N\}$ D-HMQC processing while no zero-filling for ^{14}N OT spectrum since no Fourier transform is applied, the corresponding ^{14}N slice appears more points than that of ^{14}N OT. Nevertheless, the intrinsic resolutions between these spectra are comparable. Fig. 3b shows that, for the non-protonated N5 site, the absolute intensity of ^{14}N OT (up) is higher than that of ^{14}N (down). Notably, the experimental time for CW-RESPDOR is only 0.7 hours, which is about 33-fold shorter than the D-HMQC experiment in Fig. 2. In contrast, for N7 site, its linewidth is broader as compared to that of ^{14}N slice. As a result, the absolute peak height of ^{14}N OT is lower despite the comparable integral intensity. Indeed, higher absolute intensity and narrower linewidth for ^{14}N OT of N7 can be achieved with the use of longer τ_{CW}, as shown in the following section. It is worth noting that for the sufficient detection efficiency, we recommend to use the ^{14}N OT rf-field with full strength (100 %); otherwise, the detection efficiency is low or even non-detected (see Fig. S4).

Quantitative distance information is encoded in the spectral intensities. In fact, ^1H-^{14}N OT CW-RESPDOR/REDOR experiment is originally introduced to measure internuclear distances between ^1H and ^{14}N. The fraction values $(1 - S'/S_0)$ are 0.17 for H7-N7, 0.14 for NH_3-NH_3, 0.07 for NH_3-N5, 0.11 for H6-N7 and 0.13 for H6-N5 (as shown by numbers besides these cross peaks in Fig. 3a). Although these values give qualitative measure of internuclear distances, full fraction curve to τ_{mix} allows precise determination of distances. Indeed, 3D ^1H-^{14}N dipolar/^{14}N OT/^1H correlation experiment can easily be conducted by observing CW-RESPDOR spectra with incrementing τ_{mix}.

a) $^1H/\{^{14}N\ OT\}$ CW-RESPDOR   b) 6.5 ppm

Figure 3. Hist-B: a) the 2D ^{1}H-^{14}N OT correlation map by the CW-RESPDOR experiment. While τ_{mix} and τ_{CW} were fixed at 0.768 ms and 0.128 ms, respectively, the ^{14}N OT offset was incremented from -1600 to -500 ppm with a step of 20 ppm. The number of scans was 9, thus the experimental time is 0.7 hours. The vertical axis on the far left presents the corresponding ^{14}N OT shift at the central band ($n = 0$). The small number besides each cross peak denotes the ($1 - S'/S_0$) value. b) Comparison between the relative intensity of ^{14}N OT shift array (up) extracted at ^{1}H chemical shift of 6.5 ppm (vertical line in a)) and the ^{14}N slice taken from Fig. 2c (down). The intensity of the ^{14}N OT shift array was scaled so that the noise is comparable to that of the ^{14}N slice.

The spectrum in Fig. 3a was obtained with a ^{14}N OT increment step of 20 ppm for similar resolution with ^{14}N spectrum in the *D*-HMQC experiment. A question arise here is whether this step is sufficient to well define ^{14}N OT shifts. The ^{14}N OT excitation bandwidth for a regular *D*-HMQC experiment can be described as $0.4/\tau_{CW}$[56]. Although our experiment is not *D*-HMQC, we expect similar relationship on the excitation bandwidth. With $\tau_{CW} = 0.128$ ms, the ^{14}N OT bandwidth is 3.125 kHz or 36 ppm; hence, a step of 20 ppm should be sufficient. To experimentally check the sufficiency, we performed the ^{1}H-^{14}N OT filtered CW-RESPDOR experiment with identical experimental conditions as Fig. 3 except a narrower ^{14}N OT shift step of 5 ppm. Despite different increment step, similar ^{14}N OT shift positions and linewidths for three N sites of Hist-B are observed (see Fig. S2). This confirms that the increment step of 20 ppm can sufficiently define the ^{14}N OT shift positions at least for this particular sample. Because the ^{14}N OT shifts in Fig. 3a are obtained at the second SSB ($n = -2$), we calculate the ^{14}N OT shifts at the central band ($n = 0$) for the ease of comparison (the far left vertical axis in Fig. 3a). Such value should be equal to the ^{14}N shift in ppm. This is verified by comparing ^{14}N and shifted ^{14}N OT spectra in Fig. 3b, confirming that the ^{14}N OT shifts are accurately determined. In addition, the quadrupolar product (P_Q) can be determined. We subtract the ^{14}N OT shift at the central band ($n = 0$) to the ^{15}N isotropic chemical shift (taken from CPMAS). The shift difference is the ^{14}N quadrupolar induced shift and is given by[29]:

$$\Delta = (3/40)(P_Q/v_0)^2 \times 10^6 \tag{1}$$

where Δ and v_0 denote the shift difference (in ppm) and the ^{14}N Larmor frequency, respectively, whereas P_Q is the quadrupolar product and is given by:

$$P_Q = C_Q\sqrt{[1 + (\eta_Q^2/3)]} \tag{2}$$

where C_Q and η_Q denote the quadrupolar coupling constant and the quadrupolar asymmetry parameter, respectively.

Table 1 compares the calculated ^{14}N P_Q(s) from our work with experimental P_Q in the literature[66]. These values are in good agreement, confirming again the accuracy of ^{14}N OT shifts; or in other words, the validity of the ^{1}H-^{14}N OT CW-RESPDOR experiment.

Table 1. Hist-B: comparison between calculated ^{14}N P_Q(s) and those in the literature (unit: MHz).

|	Calculated P_Q	Experimental P_Q (*)
N7	1.55	1.62
NH$_3$	1.28	1.31
N5	3.30	3.37

*: only C_Q and η_Q were provided in the previous work[66]. The experimental P_Q was calculated by Eq. 2

4.3.   Effect of ^{14}N OT CW pulse length

Our previous work showed that τ_{CW} directly affects the saturation/inversion extent of ^{14}N OT in CW-REDOR experiment; hence, S' and $(S_0 - S')$ intensities depend on τ_{CW}[62]. To further examine such dependence, we performed four 2D ^{1}H-^{14}N OT CW-RESPDOR experiments at τ_{CW} of 0.064, 0.128, 0.192, and 0.256 ms (2D spectra in Fig. S3). We note here that the S_0 and S' signals are alternatively collected at every ^{14}N OT frequency to reduce the t_1-noise that is associated with long term stability despite doubling the experimental time. Fig. 4 shows the ^{14}N OT shift array of N7 (a), **NH$_3$** (b), and N5 (c) extracted from the corresponding ^{1}H of 14.3 ppm (H7), 9.6 ppm (N**H$_3$**), and 6.5 ppm (H6) (vertical lines in Fig. S3) at different τ_{CW}. Notably, we observe in Fig. 4 that the $(S_0 - S')$ intensities for N7 and **NH$_3$** still increase at longer τ_{CW} whereas that of N5 reaches maximum at τ_{CW} of 0.128 ms. The REDOR effect is maximized when the ^{14}N OT pulse is an inversion pulse; hence, the behaviors of different N sites with respect to τ_{CW} can be explained by the flip angle. Because the flip angle depends on the quadrupolar coupling via the nutation field, our explanation can rely on P_Q. Since N7 and **NH$_3$** have similar P_Q (see Table 1), their ^{14}N OT nutation fields, thus flip angles, are also similar. On the other hand, the larger P_Q of N5 than those of N7 and **NH$_3$** generates stronger nutation ^{14}N OT field; thus, it needs shorter τ_{CW} for achieving an inversion, leading to the highest $(S_0 - S')$ intensity. We have to remind that the ^{14}N OT nutation field is

not only proportional to the size of quadrupolar coupling but also inversely proportional to the Larmor frequency. This means that the optimal τ_{CW} also depends on the B_0 magnetic field. Because Hist-B consists of three N sites with different P_Q, the optimum τ_{CW} for each site is different from each other. Hence, for sufficient $(S_0 - S')$ intensities for all three sites with ^{14}N P_Q ranging between $1 - 4$ MHz, the τ_{CW} should be around 0.128 or longer than 0.256 ms at a magnetic field of 14.1 T. However, it is advisable to use the τ_{CW} values between 0.128 and 0.192 ms that is optimal for ^{14}N sites with $P_Q = 3 - 4$ MHz, whereas the ^{14}N sites with smaller P_Q are also clearly observed under this condition despite the reduced intensities. This important result indicates that the optimization of τ_{CW} is not strictly required for our working system. Nevertheless, we recommend to conduct the optimizations once using a standard sample like Hist-B at the working B_0 and B_1 magnetic fields.

Next we consider the full width at half maximum (FWHM). The linewidth can be described as a convolution of natural linewidth and excitation bandwidth. The natural linewidth of ^{14}N OT is mainly governed by the second-order quadrupolar broadening that is proportional to the square of P_Q. Therefore, we observe a narrower FWHM for a smaller P_Q at the fixed τ_{CW} as shown in Fig. 4. The ^{14}N OT excitation bandwidth is inversely proportional to τ_{CW}, explaining why we also observe a narrower FWHM for a longer τ_{CW} at a specific N site in Fig. 4. Understanding the effect of τ_{CW} on the intensity and FWHM, we then go back the ^{14}N OT linewidth of N7 in Fig. 4. With P_Q of 1.5 MHz, higher intensity and narrower ^{14}N OT linewidth can be achieved at longer τ_{CW}. The spectral width (FWHM of 45 ppm with τ_{CW} of 0.256 ms, see Fig. 4a) is approaching that of ^{14}N (FWHM of 24 ppm, see Fig. 2c).
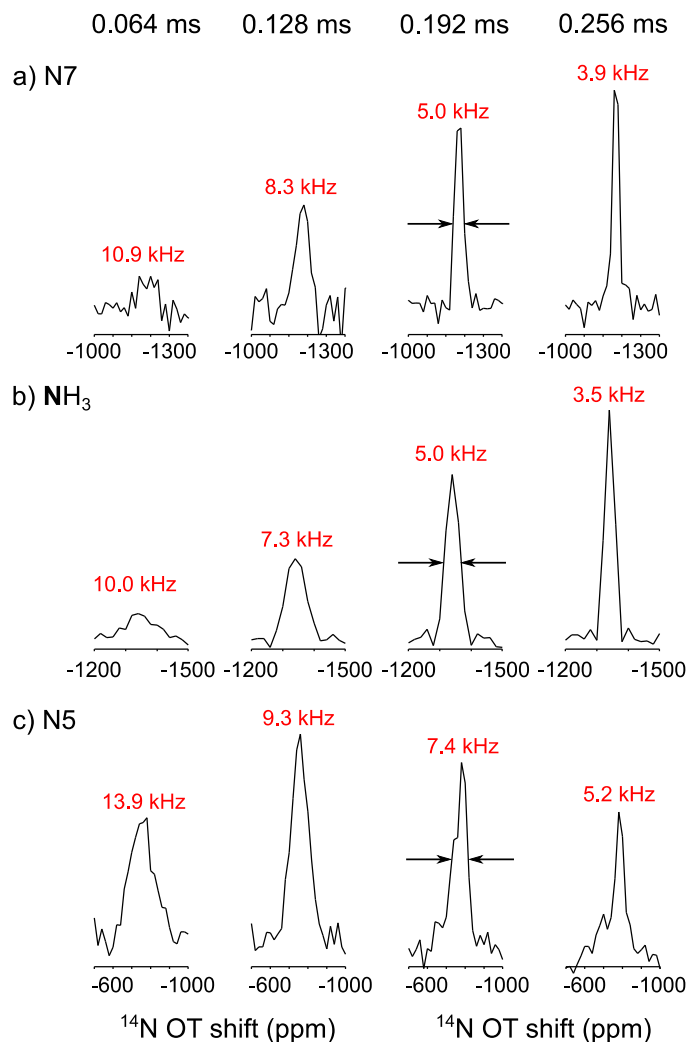
Figure 4. Hist-B: the $(S_0 - S')$ intensities for ^{14}N OT shift array of N7 (a), **N**H$_3$ (b), and N5 (c) at τ_{CW} of 0.064 ms, 0.128 ms, 0.192 ms, and 0.256 ms (from left to right). Both S_0 and S' were alternatively collected at every ^{14}N OT frequency. The remaining experimental parameters were the same and identical to those in Fig. 3a. The ^{14}N OT shift arrays of N7, **N**H$_3$, and N5 are extracted from the 2D ^{1}H-^{14}N OT spectra at ^{1}H chemical shift of 14.3 ppm (H7), 9.6 ppm (N**H$_3$**), and 6.5 ppm (H6) (vertical lines in Fig. S3), respectively. The number above each peak presents the FWHM.

4.4. ^{1}H/{^{14}N} D-HMQC and ^{1}H-^{14}N OT CW-RESPDOR experiments: AlaAla

As stated previously, the remote H6-N7 and H8-N7 correlations are clearly observed while this is not the case for H6-N5 correlation despite their similar H-N distances. We explained it due to the smaller P_Q of

N7 as compared to that of N5 (1.6 MHz and 3.3 MHz, respectively, (see Table 1)). It is expected that these difficulties often appear, since the typical C_Q value for the amide NH is about $3 - 4$ MHz. To verify this explanation, we further performed experiments on AlaAla, which consists of two N sites (NH_3 with P_Q of about 1.3 MHz and NH with P_Q of about 3.3 MHz).

Fig. 5a presents the 2D ^{1}H/{^{14}N} D-HMQC spectrum recorded at τ_{mix} of 1.536 ms (8 loops of SR4). We clearly observe weaker signal of remote C**H**(2)-**N**H correlation as compared to that of the C**H**(1)-**N**H$_3$ in spite of having similar H-N distances (2.00 and 1.97 Å, respectively). This is similar to the case of H6-N5 and H6-N7/H8-N7 correlations of Hist-B. Such observation verifies our explanation that the intensity difference when distances are similar results from P_Q values.

To clearly observe the C**H**(2)-**N**H correlation with enhanced intensity, we performed the ^{1}H-^{14}N OT CW-RESPDOR experiment. Since the P_Q of NH is about 3.3 MHz, we set τ_{CW} to 0.128 ms to favor this site instead of NH$_3$ site. Fig. 5b shows the much stronger C**H**(2)-**N**H correlation as compared to the C**H**(1)-**N**H$_3$. We note the weakened correlation of C**H**(1)-**N**H$_3$ is due to the use of τ_{CW} of 0.128 ms. To evaluate the efficiency of detecting C**H**(2)-**N**H correlation between D-HMQC and CW-RESPDOR, we extracted a ^{14}N slice and ^{14}N OT shift array at ^{1}H chemical shift of 4.9 ppm in Figs. 5a and 5b, respectively (vertical lines), and compare them together. Again, the ^{14}N OT shift array needs to be rescaled so that the noise between the two are comparable for the ease of comparison. In addition, the intrinsic resolution for ^{14}N and ^{14}N OT dimensions were set to similar each other (22.5 ppm for ^{1}H/{^{14}N} D-HMQC and 20 ppm for ^{1}H/{^{14}N OT} CW-RESPDOR). Fig. 5c shows the larger intensity of NH by ^{1}H-^{14}N OT CW-RESPDOR than that by ^{1}H/{^{14}N} D-HMQC despite the 17-fold shorter experimental time. In conclusion, ^{1}H-^{14}N OT CW-RESPDOR is a preferable method for detecting ^{1}H-^{14}N remote correlations for ^{14}N site having a large quadrupolar coupling.

14
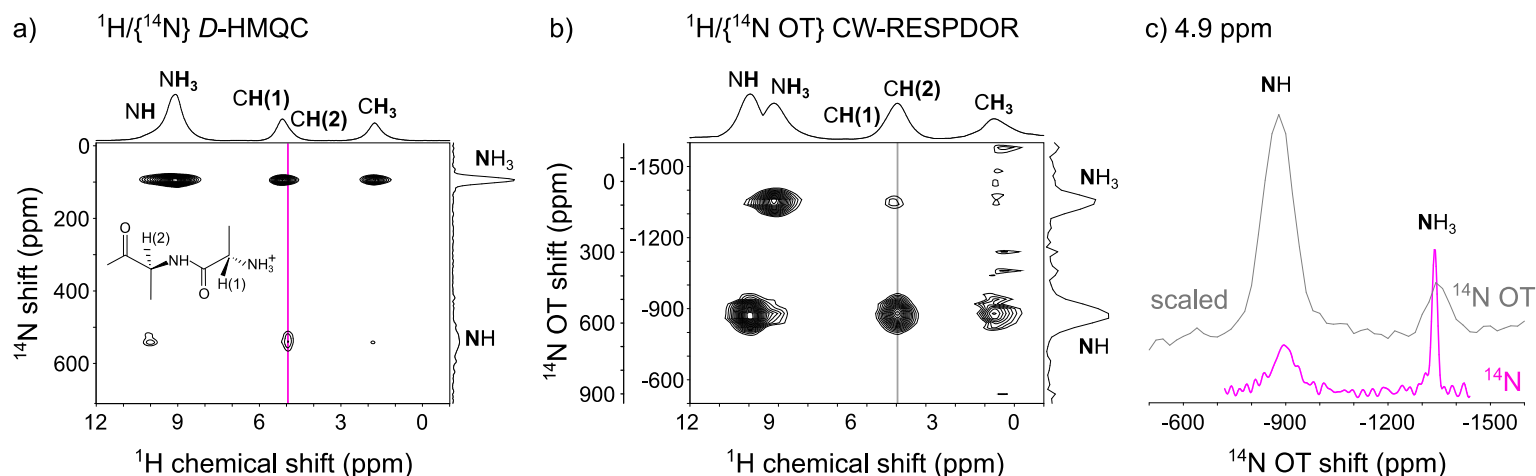
Figure 5. AlaAla: a) the 2D ^{1}H/{^{14}N} D-HMQC spectrum, recorded with 144 scans, 32 t_1 points, and rotor-synchronized t_1 increment of 32.0 μs. The ^{14}N (offset and pulse length) and $τ_{mix}$, were set to (350 ppm and 9 μs) and 1.536 ms, respectively. The experimental time was about 5.1 hour. The States-TPPI method was employed for the quadrature detection along the indirect dimension[65]. The chemical structure of AlaAla is presented. b) the 2D ^{1}H-^{14}N OT correlation map by the CW-RESPDOR experiment. The experimental conditions were identical to those in Fig. 3a except the recycling delay of 2 s. The experimental time is 0.3 hours. The vertical axis on the far left presents the corresponding ^{14}N OT shift at the central band ($n = 0$). c) Comparison between the absolute intensity of ^{14}N OT shift array (up) and the ^{14}N slice (down), all extracted at ^{1}H chemical shift of 4.9 ppm (vertical lines in a,b)). The intensity of the ^{14}N OT shift array is scaled so that the noise is comparable to that of the ^{14}N slice.

4.5.　Application

In this section, we performed ^{1}H-^{14}N OT CW-RESPDOR experiment to distinguish Hist-A and Hist-B. In a previous work, the regular ^{1}H/{^{14}N} D-HMQC experiment failed to distinguish these two polymorphs as their 2D spectra are similar[63].

Figs. 6a and 6d show the intermolecular locations of His-A and Hist-B for the shortest H8-N5 distances (3.09 and 2.69 Å), respectively. Figs. 6b and 6e show the ^{1}H single-pulse spectra whereas Fig. 6c and 6f show the corresponding 2D ^{1}H-^{14}N OT correlation maps for His-A and Hist-B, respectively. On top of the 2D spectra are the 1D ^{1}H spectra extracted at the non-protonated ^{14}N OT at -760 ppm (dashed

lines in Figs. 6c and 6f). By comparing these two ^{1}H spectra with the corresponding ^{1}H single-pulse spectra in Figs. 6b and 6e, we observe that for Hist-A, only H6 correlates to N5 whereas for Hist-B, both H6 and H8 correlate to N5. These correlations are consistent with the crystal structures of both polymorphs. Such different correlations of ^{1}Hs to the non-protonated N5 site unambiguously distinguish these two polymorphs.
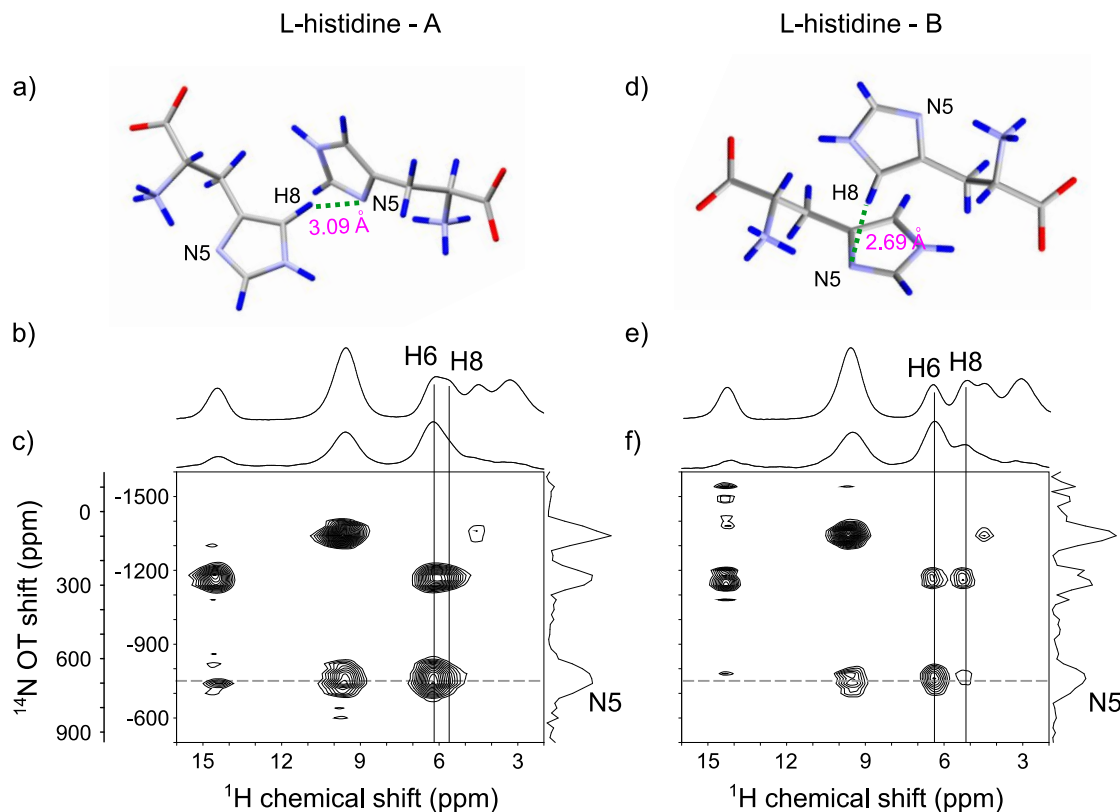
Figure 6. Hist-A (left) and Hist-B (right): a,d) intermolecular locations for the shortest H8-N5 distance. The blue, grey, violet, and red atoms denote proton, carbon, nitrogen, and oxygen, respectively. b,e) The ^{1}H single-pulse spectra and c,f) the 2D ^{1}H-^{14}N OT correlation maps. On top of the 2D spectra in (c,f) are the 1D ^{1}H spectra extracted at ^{14}N OT shift of -760 ppm (the dashed lines) for comparing with ^{1}H spectra in (b,e), respectively. The experimental conditions were identical to those in Fig. 3a. The H6 and H8 chemical shifts are presented by the vertical lines in (c,f) and the ^{14}N OT shift at the central band (n = 0) is presented by the axis in the far left in c).

5. Conclusion

We have demonstrated an approach to detect ^{1}H-^{14}N remote correlations even when ^{14}N site has a large quadrupolar coupling by the ^{1}H-^{14}N OT CW-RESPDOR experiment on Hist-B and AlaAla. The obtained 2D spectrum provides (i) one-bond and remote ^{1}H-^{14}N correlations, which allows the structural investigations and (ii) the second SSB ^{14}N OT shifts, which allows the calculations of the ^{14}N shifts, thus the ^{14}N P_Q values. The correlations of ^{1}H to the non-protonated ^{14}N site help unambiguously distinguish the two polymorphs His-A and His-B. We have presented a sample-independent estimation of τ_{mix} for the efficient detection of ^{1}H-^{14}N remote correlations. We have also investigated the effect of τ_{CW}. It has shown that for a system where ^{14}N P_Q ranges between $1 - 4$ MHz, τ_{CW} should be set between $0.128 - 0.192$ ms at the magnetic field of 14.1 T and rf-field strength of 125 kHz. These τ_{CW} values provide sufficient intensity for ^{14}N site with P_Q of $3 - 4$ MHz while ^{14}N site with smaller P_Q (about 1 MHz) appears with reduced intensities. The results on τ_{mix} and τ_{CW} have made our experiment easy to implement since almost no optimization is required. This experiment will potentially find many applications in biology, chemistry, and pharmacy field.

Acknowledgement

Conflicts of interest

There are no conflicts of interest to declare.

References

1   G. E. Martin and A. J. Williams, Long-Range ^{1}H-^{15}N Heteronuclear Shift Correlation, *Annual Reports on NMR Spectroscopy*, 2005, **55**, 1–119.

2   S. M. Althaus, K. Mao, J. A. Stringer, T. Kobayashi and M. Pruski, Indirectly detected heteronuclear correlation solid-state NMR spectroscopy of naturally abundant ^{15}N nuclei, *Solid State Nuclear Magnetic Resonance*, 2014, **57–58**, 17–21.

3   S. Cavadini, A. Lupulescu, S. Antonijevic and G. Bodenhausen, Nitrogen-14 NMR spectroscopy using residual dipolar splittings in solids., *J. Am. Chem. Soc.*, 2006, **128**, 7706–7707.

4   Z. Gan, Measuring amide nitrogen quadrupolar coupling by high-resolution ^{14}N/^{13}C NMR correlation under magic-angle spinning, *Journal of the American Chemical Society*, 2006, **128**, 6040–6041.

5   S. Cavadini, S. Antonijevic, A. Lupulescu and G. Bodenhausen, Indirect detection of nitrogen-14 in solid-state NMR spectroscopy, *ChemPhysChem*, 2007, **8**, 1363–1374.

6   S. Cavadini, S. Antonijevic, A. Lupulescu and G. Bodenhausen, Indirect detection of nitrogen-14 in solids via protons by nuclear magnetic resonance spectroscopy, *Journal of Magnetic Resonance*, 2006, **182**, 168–172.

7   S. Cavadini, A. Abraham and G. Bodenhausen, Proton-detected nitrogen-14 NMR by recoupling of heteronuclear dipolar interactions using symmetry-based sequences, *Chemical Physics Letters*, 2007, **445**, 1–5.

8   Z. Gan, J. P. Amoureux and J. Trébosc, Proton-detected ^{14}N MAS NMR using homonuclear decoupled rotary resonance, *Chemical Physics Letters*, 2007, **435**, 163–169.

9   S. Cavadini, V. Vitzthum, S. Ulzega, A. Abraham and G. Bodenhausen, Line-narrowing in proton-detected nitrogen-14 NMR, *Journal of Magnetic Resonance*, 2010, **202**, 57–63.

10   S. Cavadini, Indirect detection of nitrogen-14 in solid-state NMR spectroscopy, *Progress in Nuclear Magnetic Resonance Spectroscopy*, 2010, **56**, 46–77.

11   Y. Nishiyama, Y. Endo, T. Nemoto, H. Utsumi, K. Yamauchi, K. Hioka and T. Asakura, Very fast magic angle spinning (1)H-(14)N 2D solid-state NMR: sub-micro-liter sample data collection in a few minutes., *Journal of magnetic resonance (San Diego, Calif. : 1997)*, 2011, **208**, 44–8.

12   V. Vitzthum, M. A. Caporini, S. Ulzega and G. Bodenhausen, Broadband excitation and indirect detection of nitrogen-14 in rotating solids using Delays Alternating with Nutation (DANTE), *Journal of Magnetic Resonance*, 2011, **212**, 234–239.

13   V. Vitzthum, M. A. Caporini, S. Ulzega, J. Trébosc, O. Lafon, J. P. Amoureux and G. Bodenhausen, Uniform broadband excitation of crystallites in rotating solids using interleaved sequences of delays alternating with nutation, *Journal of Magnetic Resonance*, 2012, **223**, 228–236.

14   X. Lu, J. Trébosc, O. Lafon, D. Carnevale, S. Ulzega, G. Bodenhausen and J. P. Amoureux, Broadband excitation in solid-state NMR using interleaved DANTE pulse trains with N pulses per rotor period, *Journal of Magnetic Resonance*, 2013, **236**, 105–116.

15   A. J. Pell, K. J. Sanders, S. Wegner, G. Pintacuda and C. P. Grey, Low-power broadband solid-state MAS NMR of 14N, *Journal of Chemical Physics*, , DOI:10.1063/1.4983220.

16   Y. Li, J. Trébosc, B. Hu, M. Shen, J. P. Amoureux and O. Lafon, Indirect detection of broad spectra in solid-state NMR using interleaved DANTE trains, *Journal of Magnetic Resonance*, 2018, **294**, 101–114.

17   A. G. M. Rankin, J. Trébosc, P. Paluch, O. Lafon and J. P. Amoureux, Evaluation of excitation schemes for indirect detection of ^{14}N via solid-state HMQC NMR experiments, *Journal of Magnetic Resonance*, 2019, **303**, 28–41.

18   R. Aleksis and A. J. Pell, Low-power synchronous helical pulse sequences for large anisotropic interactions in MAS NMR: Double-quantum excitation of ^{14}N, *Journal of Chemical Physics*, , DOI:10.1063/5.0030604.

19   A. Brinkmann and A. P. M. Kentgens, Proton-selective O-17-H-1 distance measurements in fast magic-angle-spinning solid-state NMR spectroscopy for the determination of hydrogen bond lengths, *Journal Of The American Chemical Society*, 2006, **128**, 14758–14759.

20   X. Lu, O. Lafon, J. Trébosc, G. Tricot, L. Delevoye, F. Méar, L. Montagne and J. P. Amoureux, Observation of proximities between spin-1⁄2 and quadrupolar nuclei: Which heteronuclear dipolar recoupling method is preferable?, *The Journal of Chemical Physics*, 2012, **137**, 144201-1-144201–16.

21   M. Shen, J. Trébosc, O. Lafon, F. Pourpoint, B. Hu, Q. Chen and J. P. Amoureux, Improving the resolution in proton-detected through-space heteronuclear multiple quantum correlation NMR spectroscopy, *Journal of Magnetic Resonance*, 2014, **245**, 38–49.

22   F. A. Perras, T. W. Goh, L. L. Wang, W. Huang and M. Pruski, Enhanced [1]H-X D-HMQC performance through improved 1 H homonuclear decoupling, *Solid State Nuclear Magnetic Resonance*, 2019, **98**, 12–18.

23   D. Carnevale, X. Ji and G. Bodenhausen, Double cross polarization for the indirect detection of nitrogen-14 nuclei in magic angle spinning NMR spectroscopy, *Journal of Chemical Physics*, 2012, **147**, 184201, DOI:10.1063/1.5000689.

24   J. A. Jarvis, M. Concistre, I. M. Haies, R. W. Bounds, I. Kuprov, M. Carravetta and P. T. F. Williamson, Quantitative analysis of ^{14}N quadrupolar coupling using ^{1}H detected ^{14}N solid-state NMR, *Physical Chemistry Chemical Physics*, 2019, **21**, 5941–5949.

25   I. Hung and Z. Gan, High-Resolution NMR of S = 3/2 Quadrupole Nuclei by Detection of Double-Quantum Satellite Transitions via Protons, *Journal of Physical Chemistry Letters*, 2020, **11**, 4734–4740.

26   I. Hung, P. Gor'kov and Z. Gan, Efficient and sideband-free [1]H-detected ^{14}N magic-angle spinning NMR, *Journal of Chemical Physics*, , DOI:10.1063/1.5126599.

27   A. S. Tatton, J. P. Bradley, D. Iuga and S. P. Brown, [14]N-^{1}H heteronuclear multiple-quantum correlation magic-angle spinning NMR spectroscopy of organic solids, *Zeitschrift fur Physikalische Chemie*, 2012, **226**, 1187–1203.

28   A. S. Tatton, T. N. Pham, F. G. Vogt, D. Iuga, A. J. Edwards and S. P. Brown, Probing intermolecular interactions and nitrogen protonation in pharmaceuticals by novel ^{15}N-edited and 2D [14]N- [1]H

solid-state NMR, *CrystEngComm*, 2012, **14**, 2654–2659.

29   A. S. Tatton, T. N. Pham, F. G. Vogt, D. Iuga, A. J. Edwards and S. P. Brown, Probing hydrogen bonding in cocrystals and amorphous dispersions using [14]N-^{1}H HMQC solid-state NMR, *Molecular Pharmaceutics*, 2013, **10**, 999–1007.

30   S. P. Brown, Nitrogen-proton correlation experiments of organic solids at natural isotopic abundance, *eMagRes*, 2014, **3**, 243–254.

31   M. K. Pandey, J. P. Amoureux, T. Asakura and Y. Nishiyama, Sensitivity enhanced ^{14}N/^{14}N correlations to probe inter-beta-sheet interactions using fast magic angle spinning solid-state NMR in biological solids, *Physical Chemistry Chemical Physics*, 2016, **18**, 22583–22589.

32   G. N. Manjunatha Reddy, M. Malon, A. Marsh, Y. Nishiyama and S. P. Brown, Fast magic-angle spinning three-dimensional nmr experiment for simultaneously probing H-H and N-H proximities in solids, *Analytical Chemistry*, 2016, **88**, 11412–11419.

33   A. S. Tatton, H. Blade, S. P. Brown, P. Hodgkinson, L. P. Hughes, S. O. N. Lill and J. R. Yates, Improving Confidence in Crystal Structure Solutions Using NMR Crystallography: The Case of β-Piroxicam, *Crystal Growth & Design*, 2018, acs.cgd.8b00022.

34   D. Carnevale, B. Grosjean and G. Bodenhausen, Dipolar couplings in solid polypeptides probed by ^{14}N NMR spectroscopy, *Communications Chemistry*, 2018, **1**, 1–9.

35   Y. Hong, T. Asakura and Y. Nishiyama, 3D ^{14}N/[1]H Double Quantum/[1]H Single Quantum Correlation Solid-State NMR for Probing Parallel and Anti-Parallel Beta-Sheet Arrangement of Oligo-Peptides at Natural Abundance, *ChemPhysChem*, 2018, **32**, 60–73.

36   A. V. Wijesekara, A. Venkatesh, B. J. Lampkin, B. VanVeller, J. W. Lubach, K. Nagapudi, I. Hung, P. L. Gor'kov, Z. Gan and A. J. Rossini, Fast Acquisition of Proton-Detected HETCOR Solid-State NMR Spectra of Quadrupolar Nuclei and Rapid Measurement of NH Bond Lengths by Frequency Selective HMQC and RESPDOR Pulse Sequences, *Chemistry – A European Journal*, 2020, **26**, 7881–7888.

37   A. Venkatesh, I. Hung, K. C. Boteju, A. D. Sadow, P. L. Gor'kov, Z. Gan and A. J. Rossini, Suppressing [1]H Spin Diffusion in Fast MAS Proton Detected Heteronuclear Correlation Solid-State NMR Experiments, *Solid State Nuclear Magnetic Resonance*, 2020, **105**, 101636.

38   T. Kobayashi, Y. Nishiyama and M. Pruski, Chapter 1. Heteronuclear correlation solid-state NMR spectroscopy with indirect detection under fast magic-angle spinning. *Modern Methods in Solid-state NMR: A Practitioner's Guide*. Hodgkinson, P., Ed. New Developments in NMR; Royal Society of Chemistry: Cambridge 2018; ISBN 978-1-78262-854-5, pp. 1–38.

39   Z. Gan, Measuring multiple carbon-nitrogen distances in natural abundant solids using R-RESPDOR NMR, *Chemical Communications*, 2006, 4712–4714.

40   L. Chen, Q. Wang, B. Hu, O. Lafon, J. Trébosc, F. Deng and J. P. Amoureux, Measurement of hetero-nuclear distances using a symmetry-based pulse sequence in solid-state NMR, *Physical Chemistry Chemical Physics*, 2010, **12**, 9395–9405.

41   L. Chen, X. Lu, Q. Wang, O. Lafon, J. Trébosc, F. Deng and J. P. Amoureux, Distance measurement between a spin-1/2 and a half-integer quadrupolar nuclei by solid-state NMR using exact analytical expressions, *Journal of Magnetic Resonance*, 2010, **206**, 269–273.

42   N. T. Duong, F. Rossi, M. Makrinich, A. Goldbourt, M. R. Chierotti, R. Gobetto and Y. Nishiyama, Accurate ^{1}H-^{14}N distance measurements by phase-modulated RESPDOR at ultra-fast MAS, *Journal of Magnetic Resonance*, 2019, **308**, 106559.

43   D. Bernasconi, S. Bordignon, F. Rossi, E. Priola, C. Nervi, R. Gobetto, D. Voinovich, D. Hasa, N. T. Duong, Y. Nishiyama and M. R. Chierotti, Selective Synthesis of a Salt and a Cocrystal of the Ethionamide–Salicylic Acid System, *Crystal Growth & Design*, 2020, **20**, 906–915.

44   S. S. Nagarkar, H. Kurasho, N. T. Duong, Y. Nishiyama, S. Kitagawa and S. Horike, Crystal melting and glass formation in copper thiocyanate based coordination polymers, *Chemical Communications*, 2019, **55**, 5455–5458.

45   G. Qi, Q. Wang, J. Xu, J. Trébosc, O. Lafon, C. Wang, J. P. Amoureux and F. Deng, Synergic Effect of Active Sites in Zinc-Modified ZSM-5 Zeolites as Revealed by High-Field Solid-State NMR Spectroscopy, *Angewandte Chemie - International Edition*, 2016, **55**, 15826–15830.

46   P. Gao, Q. Wang, J. Xu, G. Qi, C. Wang, X. Zhou, X. Zhao, N. Feng, X. Liu and F. Deng, Brønsted/Lewis Acid Synergy in Methanol-to-Aromatics Conversion on Ga-Modified ZSM-5 Zeolites, As Studied by Solid-State NMR Spectroscopy, *ACS Catalysis*, 2018, **8**, 69–74.

47   T. Matsunaga, J. Kanazawa, T. Ichikawa, M. Harada, Y. Nishiyama, N. T. Duong, T. Matsumoto, K. Miyamoto and M. Uchiyama, α-Cyclodextrin Encapsulation of Bicyclo[1.1.1]pentane Derivatives: A Storable Feedstock for Preparation of [1.1.1]Propellane, *Angewandte Chemie - International Edition*, 2021, **60**, 2578–2582.

48   W. Gao, G. Qi, Q. Wang, W. Wang, S. Li, I. Hung, Z. Gan, J. Xu and F. Deng, Dual Active Sites on Molybdenum/ZSM-5 Catalyst for Methane Dehydroaromatization: Insights from Solid-State NMR Spectroscopy, *Angewandte Chemie - International Edition*, 2021, **60**, 10709–10715.

49   M. Bloom and M. A. LeGros, Direct detection of two-quantum coherence, *Canadian Journal of Physics*, 1986, **64**, 1522–1528.

50   R. Tycko and S. J. Opella, High-Resolution 14N Overtone Spectroscopy: An Approach to Natural Abundance Nitrogen NMR of Oriented and Polycrystalline Systems, *Journal of the American Chemical Society*, 1986, **108**, 3531–3532.

51   R. Tycko and S. J. Opella, Overtone NMR spectroscopy, *The Journal of Chemical Physics*, 1987, **86**, 1761.

52   L. A. O'Dell and C. I. Ratcliffe, ^{14}N magic angle spinning overtone NMR spectra, *Chemical Physics Letters*, 2011, **514**, 168–173.

53   L. A. O'Dell and A. Brinkmann, ^{14}N overtone NMR spectra under magic angle spinning: Experiments and numerically exact simulations, *Journal of Chemical Physics*, , DOI:10.1063/1.4775592.

54   L. O'Dell, ^{14}N Overtone Magic Angle Spinning NMR, *Annual Reports on NMR Spectroscopy*, 2015, **86**, 211–236.

55   Z. Gan, I. Hung, Y. Nishiyama, J. P. Amoureux, O. Lafon, H. Nagashima, J. Trébosc and B. Hu, ^{14}N overtone nuclear magnetic resonance of rotating solids, *Journal of Chemical Physics*, , DOI:10.1063/1.5044653.

56   Y. Nishiyama, M. Malon, Z. Gan, Y. Endo and T. Nemoto, Proton-nitrogen-14 overtone two-dimensional correlation NMR spectroscopy of solid-sample at very fast magic angle sample spinning., *Journal of magnetic resonance (San Diego, Calif. : 1997)*, 2013, **230**, 160–4.

57   L. O'Dell, R. He and J. Pandohee, Identifying H–N proximities in solid-state NMR using ^{14}N overtone irradiation under fast MAS, *CrystEngComm*, 2013, **15**, 8657–8667.

58   I. M. Haies, J. A. Jarvis, H. Bentley, I. Heinmaa, I. Kuprov, P. T. F. Williamson and M. Carravetta, ^{14}N overtone NMR under MAS: signal enhancement using symmetry-based sequences and novel simulation strategies, *Physical Chemistry Chemical Physics*, 2015, **17**, 6577–6587.

59   M. Shen, Q. Chen and B. Hu, Composite pulses in directly and indirectly detected ^{14}N MAS overtone spectroscopy, *Solid State Nuclear Magnetic Resonance*, 2017, **84**, 132–136.

60   C. P. Grey and A. J. Vega, Determination of the Quadrupole Coupling Constant of the Invisible Aluminum Spins in Zeolite HY with ^{1}H/^{27}Al TRAPDOR NMR, *Journal of the American Chemical Society*, 1995, **117**, 8232–8242.

61   H. Koller, T. Uesbeck, M. R. Hansen and M. Hunger, Characterizing the First and Second ^{27}Al Neighbors of Brønsted and Lewis Acid Protons in Zeolites and the Distribution of ^{27}Al Quadrupolar Couplings by ^{1}H{^{27}Al} Offset REAPDOR, *The Journal of Physical Chemistry C*, 2017, 121, 25930-25940, DOI: 10.1021/acs.jpcc.7b09544.

62   N. T. Duong, Z. Gan and Y. Nishiyama, Selective ^{1}H-^{14}N Distance Measurements by ^{14}N Overtone Solid-State NMR Spectroscopy at Fast MAS, *Frontiers in Molecular Biosciences*, 2021, **8**, 645347, DOI:10.3389/fmolb.2021.645347.

63   T. Oikawa, M. Okumura, T. Kimura and Y. Nishiyama, Solid-state NMR meets electron diffraction: Determination of crystalline polymorphs of small organic microcrystalline samples, *Acta Crystallographica Section C: Structural Chemistry*, 2017, **73**, 219–228.

64   I. Hung, P. Gor'kov and Z. Gan, Using the heteronuclear Bloch-Siegert shift of protons for B_1 calibration of insensitive nuclei not present in the sample, *Journal of Magnetic Resonance*, 2020, **310**, 106636.

65   D. Marion, M. Ikura, R. Tschudin and A. Bax, Rapid recording of 2D NMR spectra without phase cycling. Application to the study of hydrogen exchange in proteins, *Journal of Magnetic Resonance (1969)*, 1989, **85**, 393–399.

66   D. T. Edmonds and C. P. Summers, ^{14}N pure quadrupole resonance in solid amino acids, *Journal of Magnetic Resonance (1969)*, 1973, **12**, 134–142.